Original Article

Biosynthesis of Zinc Nanoparticles Using Star Anise and Evaluation of Their Antimicrobial Efficacy Against Microbes Isolated from Sheep Meat

S. S. Daoud, M. S. Mahdi

Department of Food Science, College of Agriculture, Tikrit University Iraq

Abstract

The study was conducted in the laboratories of the Food Science Department and the Central Laboratory at the College of Agriculture, Tikrit University. Its primary objective was the biosynthesis of zinc oxide nanoparticles (ZnO NPs) using star anise extract (*Illicium verum*) and the evaluation of their inhibitory effect against foodborne pathogenic bacteria, namely *Staphylococcus aureus*, *Escherichia coli*, *Pseudomonas aeruginosa*, and *Salmonella*. These microorganisms were identified through a range of morphological and biochemical tests, as well as VITEK system analysis. The green synthesis of zinc oxide nanoparticles using the aqueous star anise extract was confirmed by a clear color change in the reaction mixture. Specifically, within 20 minutes of adding the initial zinc oxide to the extract, the solution changed color from yellow to light brown, indicating the formation of nanoparticles. Further characterization using scanning electron microscopy (SEM) revealed that the biosynthesized zinc oxide nanoparticles were predominantly spherical, with particle sizes ranging from 25.4 to 78.4 nm. UV-Vis spectroscopy analysis of the aqueous extract of star anise treated with zinc oxide nanoparticles revealed a distinct absorption pattern. Upon the addition of zinc oxide nanoparticles (ZnO-NPs) to star anise, an absorption range of 280–900 nm was observed, peaking between 280 and 300 nm with an absorption rate of approximately 1.5 absorptivity units. Beyond this range, the absorption gradually decreased with increasing wavelength, approaching zero after 400 nm. Fourier transform infrared (FTIR) spectroscopy analysis of the same extract also revealed patterns. X-ray diffraction (XRD) analysis of the star anise extract treated with zinc oxide nanoparticles revealed patterns. The distinct crystalline structure indicates successful formation of nanoparticles with a defined crystalline structure. The aqueous extract of star anise alone exhibited varying antibacterial activity against bacteria isolated from meat. It showed significant inhibitory effects against *Salmonella* and *Escherichia coli*, but no significant activity was observed against *Staphylococcus aureus* or *Pseudomonas aeruginosa*. The zones of inhibition for *Salmonella* at concentrations of 125, 250, 500, and 1000 µg/ml were 1.8, 2.0, 3.8, and 3.8 cm², respectively. The compound demonstrated inhibitory activity against all tested bacterial strains. These results confirm the high antimicrobial potential of the plant-nanoparticle combination, particularly in suppressing the growth of meat-associated pathogens.

Keywords: nanocomposite, Zinc nanoparticles, Star anise, Microbes, lamb meat

Address for Correspondence

* Correspondence to: Sarah Samir Dawood, Department of Food Science, College of Agriculture, Tikrit University, Iraq. E-mail: sd230010pag@st.tu.edu.iq

Received: 2025-08-14 **Accepted:** 2025-11-12 **Published:** 2026-06-30

DOI: https://doi.org/10.32649/ajas.2025.163560.1781

How to cite this article: Daoud, S. S., and Mahdi, M. S. (2026). Biosynthesis of Zinc Nanoparticles Using Star Anise and Evaluation of Their Antimicrobial Efficacy Against Microbes Isolated from Sheep Meat. *Anbar Journal of Agricultural Sciences*, 24(2), 452-467. https://doi.org/10.32649/ajas.2025.163560.1781

Introduction

Zinc oxide nanoparticles (ZnO NPs) are white, inorganic nanoparticles (ZnO) that are widely used in food applications due to their strong antimicrobial activity. They are safe for human cells, unlike heavy metals such as lead, copper, cobalt, and cadmium, which, if present in meat, can cause food poisoning (5). They are used in food packaging to improve microbial resistance, barrier strength, and durability (7). Their antimicrobial power comes from their ability to generate ROS and alter surface properties. ZnO NPs have shown inhibitory effects against *S. aureus*, *E. coli*, *Salmonella typhimurium*, and *Klebsiella pneumoniae*, with MICs ranging from 5–15 µg/ml (9) Higher concentrations (up to 45 µg/ml) significantly increased bacterial inhibition after 4–5 hours of exposure. Nanoparticles can be synthesized via two main methods. Bottom-up approach

©Authors, 2026, College of Agriculture, University of Anbar. This is an open-access article under the CC BY 4.0 license (http://creativecommons.org/licenses/by/4.0/).

– involves atomic-level assembly through redox reactions, producing stable nanostructures using chemical or biological means **(19)**. Top-down approach – more costly, involving physical breakdown (e.g., milling) of bulk materials into nanoparticles. However, it requires high energy and often produces non-ideal surfaces **(38)**. Mechanism of Nanoparticles and Role of ZnO NPs. Nanoparticles affect bacteria through several key mechanisms. Studies show they are generally more effective against Gram-positive bacteria than Gram-negative, due to differences in cell wall structure. Gram-negative bacteria have an outer membrane rich in lipopolysaccharides and lipoproteins, which limits nanoparticle penetration. In contrast, Gram-positive bacteria have a thick peptidoglycan layer with pores that allow easier entry, leading to membrane damage and cell death **(35)**. Another major antibacterial mechanism is the generation of reactive oxygen species (ROS), such as superoxide (O_2^-), hydroxyl radicals (OH), hydrogen peroxide (H_2O_2), and singlet oxygen ($^1O_2$). While some ROS can be neutralized by bacterial enzymes, others—especially OH and $^1O_2$—cause severe oxidative stress and bacterial death **(24)**. Nanoparticles can also penetrate the bacterial membrane, disrupting internal functions by interacting with DNA and proteins **(44)**.

Materials and Methods

Reagents and Solutions:

Gram's Stain Solutions: Prepared according to **(47)**.

Normal Saline: Prepared by dissolving 8.5 g of sodium chloride (NaCl) in 1 liter of distilled water, adjusting pH to 7.2 **(6)**.

MacFarland Standard (0.5 Tube): Prepared using two solutions **(3)**:

Solution A: 1.75 g barium chloride ($BaCl_2$) dissolved in 100 mL distilled water.

Solution B: 1 mL concentrated sulfuric acid (H_2SO_4) diluted in 100 mL distilled water.

0.5 mL of solution A was added to 99.5 mL of solution B to obtain a turbidity equivalent to approximately 1.5×10^8 cells/mL.

Sample Collection:

Random fresh meat samples were collected from local markets in Tikrit, placed in sterile, refrigerated plastic containers, and transported directly to the laboratory following strict hygienic procedures for bacterial isolation.

Isolation of Microorganisms:

Ten grams of meat sample were homogenized in 90 mL normal saline to prepare serial dilutions. Then, 0.1 mL of the final dilution was spread evenly using a sterile L-shaped glass spreader on culture media plates, which were incubated inverted at 37°C for 24 hours. After colony development, individual colonies were isolated by streaking to obtain pure cultures. Bacteria were identified morphologically, microscopically, and biochemically.

Preservation of Isolates:

Bacterial isolates were stored on nutrient agar slants at 4°C and subcultured monthly on fresh media to maintain viability **(42)**.

Diagnosis using the Vitek 2 Compact System

After culturing the microorganisms, pure colonies were isolated for identification using the Vitek 2 Compact System. The following steps were followed to identify the bacterial species:

1. The nutrient agar medium was inoculated with the bacterial isolates and incubated at 37°C for 24 hours. A Kan tube was then used for diagnostic purposes and placed inside the colonies with 3 ml of normal saline solution to obtain the required density, which was then measured using a density check. 2. The tube is placed in the density check reader to measure the density level. The required density for both Gram-positive and Gram-negative bacteria is between 0.5 and 0.63. The kit is then placed inside a Kan tube on a holder for insertion into the instrument. It is then inserted through the filling door and subsequently into the loading door. Incubation is then performed by inserting the kit through the user access door. Diagnosis may take 4-6 hours to obtain the final result.

Characterization of Nanoparticles

-Ultraviolet Spectroscopy

The optical properties of zinc and titanium nanoparticles derived from star anise extract were determined using ultraviolet spectroscopy at the Research Center, University of Baghdad. The sample was prepared by taking 1 ml of the pre-prepared solution and placing it in a UV-Vis spectrometer at a wavelength of 200-800 nm, while recording the absorbance values of the zinc oxide nanoparticles and titanium nanoparticles **(13)**.

-Diagnosis using Infrared Spectroscopy

Bio-synthesized zinc oxide and titanium nanoparticles from the aqueous extract of star anise were analyzed using Fourier transform infrared spectroscopy (FTIR) within the scanning range of 4000-6000 cm^{-1} to identify the active groups present in the sample and to examine the vibrational structures of the solids. The analysis was performed at room temperature (25°C) after taking drops of the solution and placing them in the instrument's cell. The analysis was conducted at the Research Center - University of Baghdad **(15)**.

- X-ray Diffraction Microscope

Zinc and titanium oxide particles were sent to the Research Center at the University of Baghdad for X-ray diffraction (XRD) analysis. XRD is a common analytical technique used to analyze molecular and crystal structures, qualitatively identify different compounds, quantitatively determine chemical species, measure degree of crystallinity, identify homologs, and determine particle sizes **(48)**.

-Scanning Electron Microscope (SEM)

Scanning electron microscopy (SEM) was used to characterize the morphology and size of the nanoparticles at the Research Center at the University of Baghdad. The sample was prepared by adding a small droplet of the biocomposite nanoparticles to a silicon wafer, allowing it to dry, and then analyzing it using SEM. The microscope was operated at an accelerated voltage of 12.5-15 kV with different magnifications and working distances of 5-10 cm **(10)**.

Preparation of Zinc Nanocomposite with Star Anise:

Following **(8)**, 1 g of star anise powder was added to a zinc solution prepared by dissolving 1 g of zinc nanoparticles in 50 mL ion-free distilled water. The mixture was stirred magnetically at room temperature for 24 hours, then incubated with shaking at 40°C for 18 hours until a color change was observed. The precipitate was separated by centrifugation at 3000 rpm for 20 minutes, washed several times with ion-free distilled water, dried at 50°C in an oven, ground finely with a ceramic mortar, and stored in a refrigerator until use.

Measuring the inhibitory activity of nano zinc oxide solution with star anise against some Gram-positive and Gram-negative bacterial strains:

The inhibitory effect was measured following **(32)**. using the agar well diffusion method. Bacterial suspensions (*E. coli*, *Salmonella*, *Pseudomonas*, *Staphylococcus aureus*) were spread on Mueller-Hinton agar plates. Four wells of 6 mm diameter were made in each plate, and various concentrations (125, 250, 500, 1000 µg/mL) of ZnO nanoparticles with star anise, TiO_2 nanoparticles with star anise, and star anise extract alone were added. Plates were incubated at 37°C for 24 hours. Antibacterial activity was assessed by measuring the diameter of the inhibition zones around wells.

Antibiotic susceptibility testing of bacteria.

The susceptibility test was performed using the antibiotic tablet method, employing eight different antibiotics:

Cephalexin cl 30

Amikacin (Ak 10

Tetracyclin TE10

Penicillin P 10

Cefixime CFM5

Amoxicillin AX 10

Cefotaxime CTX 10

Bacitracin B 10

Statistical Analysis:

Experiments were performed under a Complete Randomized Design (CRD). Analysis of variance (ANOVA) was conducted using the General Linear Model in **(36)**. Duncan's multiple range test **(14)** was used to determine significant differences between means at $p \leq 0.05$.

Results and Discussion

Diagnosis using VITEK

The VITEK 2 Compact system demonstrated high efficiency in the automated identification of bacterial isolates obtained from meat samples. Four major contaminating species were accurately identified: *Escherichia coli*, *Staphylococcus aureus*, *Pseudomonas aeruginosa*, and *Salmonella* spp., with identification accuracy ranging between 86% and 95% in less than seven hours. *E. coli* was identified with 86% accuracy within 5.05 hours, a common meat contaminant often associated with intestinal leakage or contaminated tools during slaughter. These findings align with **(39)**, who detected *E. coli* and *S. aureus* in partially cooked chicken using VITEK 2 with 100% agreement compared to conventional methods. Similar agreement was reported by **(2)**, who identified *E. coli* from raw and ready-to-eat meats with 86% accuracy within six hours.

Staphylococcus aureus was identified with 90% confidence in 5.83 hours. This Gram-positive bacterium is commonly linked to contamination through poor handling or unsterilized equipment. These results are consistent with **(4)**, who reported *S. aureus* contamination resulting mainly from poor hygiene during meat processing. *Pseudomonas aeruginosa* was identified with 92% accuracy in 6.45 hours. This Gram-negative species thrives in moist, cold environments. Similar outcomes were reported by **(45)**, who successfully diagnosed *P. aeruginosa* from infected camel meat using the same system. *Salmonella* spp. were identified with 95% accuracy within 6.25 hours, confirming their role as a major pathogen in contaminated meat. These results match those of **(45)**, who detected *Salmonella* in camel lung samples using VITEK 2, as well as **(30)**, who reported 93% prevalence in street-sold meat, identified within 6.1 hours using the same system.

Table 1. Diagnosis of *Escherichia coli* isolation using the VITEK 2 Compact device.

Identification Information						Analysis Time: 5.05 hours								Status: Final			
Selected Organism						86% Probability Escherichia coli Bio number: 340001061765431											
ID Analysis Messages																	
Biochemical Details																	
2	AMY	+	4	PIPLC	+	5	dXYL	-	8	ADHl	-	9	BGAL	-	11	AGLU	+
13	APPA	-	14	CDEX	-	15	AspA	-	16	BGAL	-	17	AMAN	(-)	19	PHOS	-
20	LeuA	-	23	ProA	-	24	BGURr	-	25	AGAL	+	26	PyrA	-	27	BGUR	(-)
28	AlaA	-	29	TyrA	-	30	dSOR	-	31	URE	-	32	POLYB	+	37	dGAL	+
38	dRIB	+	39	lLATk	-	42	LAC	-	44	NAG	+	45	dMAL	+	46	BACI	+
47	NOVO	-	50	NC6.5	+	52	dMAN	+	53	dMNE	+	54	MBdG	-	56	PUL	+
57	dRAF	-	58	O129R	-	59	SAL	+	60	SAC	+	62	dTRE	+	63	ADH2s	-
64	OPTP	+															

Table 2. Diagnosis of *Pseudomonas aeruginosa* isolation using the VITEK 2 Compact device.

Identification Information						Analysis Time: 6.83 hours								Status: Final			
Selected Organism						89% Probability Pseudomonas aeruginosa Bio number: 4401700240000610											
ID Analysis Messages																	
Biochemical Details																	
2	APPA	-	3	ADO	-	4	PyrA	+	5	lARL	-	7	dCEL	-	9	BGAL	+
10	H2S	-	11	BNAG	-	12	AGLTp	-	13	dGLU	+	14	GGT	-	15	OFF	-
17	BGLU	+	18	dMAL	+	19	dMAN	+	20	dMNE	-	21	BXYL	-	22	BAlap	-
23	ProA	-	26	LIP	-	27	PLE	-	29	TyrA	-	31	URE	+	32	dSOR	-
33	SAC	-	34	dTAG	-	35	dTRE	+	36	CIT	-	37	MNT	-	39	5KG	-
40	lLATk	-	41	AGLU	-	42	SUCT	-	43	NAGA	-	44	AGAL	-	45	PHOS	-
46	GlyA	-	47	ODC	-	48	LDC	-	53	lHISa	-	56	CMT	+	57	BGUR	+
58	O129R	+	59	GGAA	-	61	lMLTa	-	62	ELLM	-	64	ILATa	-			

Table 3. Diagnosis of *Salmonella* isolation using the VITEK 2 Compact device.

Identification Information						Analysis Time: 5.80 hours								Status: Final			
Selected Organism						95% Probability Salmonella Bio number: 5400001000000200											
ID Analysis Messages																	
Biochemical Details																	
2	APPA	+	3	ADO	-	4	PyrA	+	5	lARL	-	7	dCEL	-	9	BGAL	+
10	H2S	-	11	BNAG	-	12	AGLTp	-	13	dGLU	-	14	GGT	-	15	OFF	-
17	BGLU	-	18	dMAL	-	19	dMAN	-	20	dMNE	-	21	BXYL	-	22	BAlap	-
23	ProA	+	26	LIP	-	27	PLE	-	29	TyrA	-	31	URE	-	32	dSOR	-
33	SAC	-	34	dTAG	-	35	dTRE	-	36	CIT	-	37	MNT	-	39	5KG	-
40	lLATk	-	41	AGLU	-	42	SUCT	-	43	NAGA	-	44	AGAL	-	45	PHOS	-
46	GlyA	-	47	ODC	-	48	LDC	-	53	lHISa	-	56	CMT	+	57	BGUR	-
58	O129R	-	59	GGAA	-	61	lMLTa	-	62	ELLM	-	64	ILATa	-			

Table 4. Diagnosis of *Staphylococcus aureus* isolation using the VITEK 2 Compact device.

Identification Information						Analysis Time: 5.83 hours								Status: Final			
Selected Organism						90% Probability Staphylococcus ausreus Bio number: 050002021720221											
ID Analysis Messages																	
Biochemical Details																	
2	AMY	-	4	PIPLC	-	5	dXYL	-	8	ADHl	+	9	BGAL	-	11	AGLU	+
13	APPA	-	14	CDEX	-	15	AspA	-	16	BGAL	-	17	AMAN	-	19	PHOS	-
20	LeuA	-	23	ProA	-	24	BGURr	-	25	AGAL	-	26	PyrA	+	27	BGUR	-
28	AlaA	-	29	TyrA	-	30	dSOR	-	31	URE	-	32	POLYB	+	37	dGAL	-
38	dRIB	+	39	lLATk	-	42	LAC	-	44	NAG	+	45	dMAL	+	46	BACI	+
47	NOVO	-	50	NC6.5	+	52	dMAN	-	53	dMNE	-	54	MBdG	-	56	PUL	-
57	dRAF	-	58	O129R	+	59	SAL	-	60	SAC	-	62	dTRE	+	63	ADH2s	-
64	OPTP	+															

Green manufacturing of nanoparticles:

Based on the results shown in **Figure (1)**, the green synthesis of zinc oxide nanoparticles using aqueous star anise extract was successful, as indicated by a visible color change from yellow to light brown within 20 minutes of adding the metal ions. This shift signals a reduction reaction between the bioactive compounds in the extract and the zinc ions, forming nanoparticles — a hallmark of eco-friendly green synthesis using plant-based materials instead of chemicals. The observed color change is primarily attributed to Surface Plasmon Resonance (SPR), which results from the reduction in particle size to the nanoscale and affects light absorption and visible spectra **(23)**. This phenomenon is supported by **(46)**, who highlighted the importance of nanoscale imaging in understanding SPR, who demonstrated its role in light emission, and, who used SPR to monitor protein layer formation on nanoparticles. The presence of phenolic and flavonoid compounds in the plant extract significantly enhanced the reduction process and nanoparticle formation.

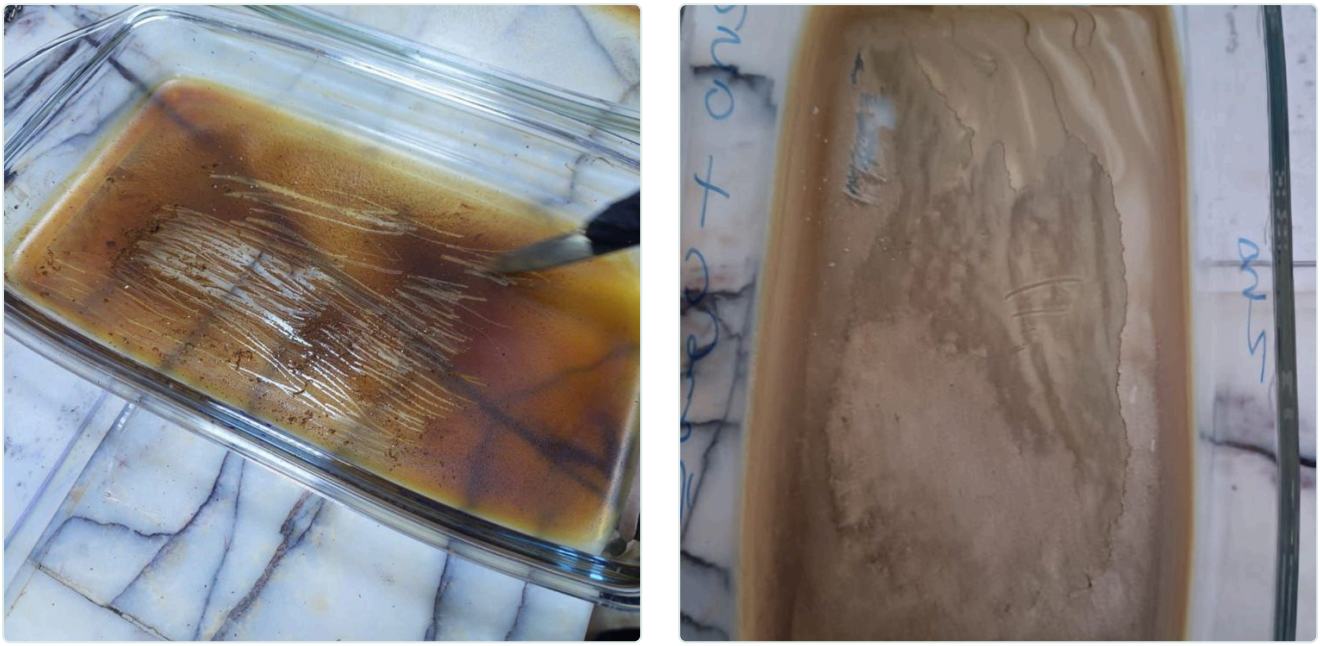

(a) Star anise extract (b) Anise extract with nano zinc oxide

Figure 1. Visual confirmation of ZnO nanoparticle formation. (a) Aqueous star anise extract (yellow). (b) The reaction mixture after 20 minutes, showing a color change to light brown, indicative of the formation of ZnO nanoparticles through the reduction of zinc ions by the plant's bioactive compounds.

Scanning electron microscope

Using scanning electron microscopy (SEM) to determine the surface morphology and structure of nanoparticles synthesized using star anise extract, the results shown in **Figure (2)** indicate that the zinc oxide (ZnO) nanoparticles were spherical, ranging in size from 25.4 to 78.4 nm. These results suggest that the type of metal particle influences the resulting particle shape and size, reflecting the ability of the active compounds in the plant extract to control particle formation. These findings are consistent with those of **(20)**, who reported that nanoparticles prepared using plant extracts exhibit size variations ranging from 25 to 130 nm, depending on the metal used and the active compounds in the extract. The researchers emphasized that this variation is related to the biosynthetic mechanism, which relies on the activity of plant compounds—particularly phenols and flavonoids—in reducing metal ions and stabilizing the formed particles. The results showed that the produced nanoparticles exhibited properties suitable for therapeutic applications, reflecting the effectiveness of green synthesis in controlling size and biological activity. The study by **(41)** supported the finding that particle size typically ranges from 20 to 140 nanometers and is influenced by several factors, including plant species, reaction temperature, and reaction time. The researchers explained that the active compounds in plant extracts directly contribute to regulating the rate of nuclear reduction and particle growth, ultimately affecting their physical dimensions. The study by **(29)** confirmed that the variation in nanoparticle size and shape depends closely on the type of plant extract used and its chemical composition, particularly its phenolic content. The researchers explained that these compounds play a pivotal role in reduction processes and in controlling particle growth and morphology, which directly impacts the morphological and functional properties of the nanoparticles. The significance of these results lies in enhancing the ability of green biofabrication to produce highly efficient nanoparticles by selecting plant extracts rich in bioactive compounds, thus ensuring precise control over the physical properties of the particles. Furthermore, data obtained from SEM images confirm that ZnO nanoparticles synthesized using anise extract are spherical and larger in size. This variation in shape and size directly impacts the physical, chemical, and functional properties of the particles, reinforcing the importance of selecting the appropriate metal and extract based on the intended application.

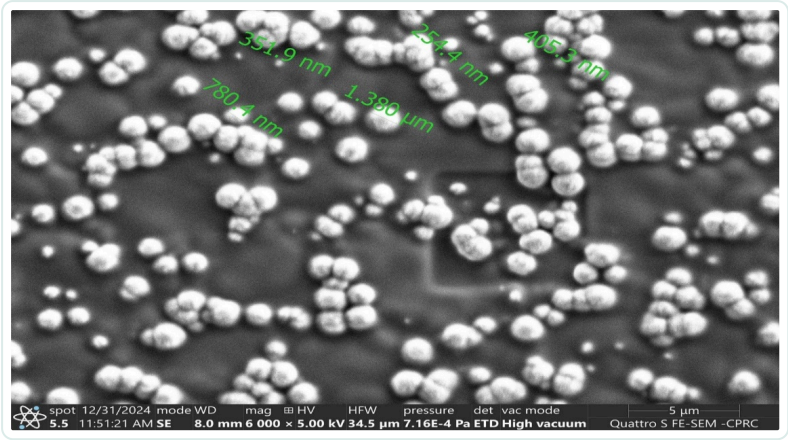

Figure 2. The size and shape of star anise extract particles are illustrated by the addition of zinc oxide nanoparticles.

UV-Visible Spectroscopy

The UV-Visible spectroscopy analysis of the aqueous extract of star anise treated with zinc oxide nanoparticles revealed a distinctive spectral absorption pattern, as shown in **Figures 3**. This analysis is an important tool for confirming the composition of the nanoparticles and determining their spectral response to light. The star anise extract supplemented with zinc oxide nanoparticles (ZnO-NPs) (**Figure 3**) exhibited an absorption range between 280 and 900 nm, peaking at a wavelength between 280 and 300 nm with an absorption rate of approximately 1.5 absorptivity units. Beyond this point, absorption gradually decreased with increasing wavelength, approaching zero after 400 nm. This indicates that the particles effectively absorb light only in the ultraviolet (UV) range, with negligible absorption in the visible range. This is evidence of the formation of stable nanoparticles with distinctive electronic properties. These results are consistent with what was indicated by both **(28) (34)**, that zinc oxide (ZnO) nanoparticles exhibit strong absorption peaks in the ultraviolet spectrum within the 280–320 nm range, which are due to electronic transitions from the valence band to the conduction band. This spectral property is a characteristic feature of semiconductor nanoparticles, as it is related to the phenomenon of quantum absorption resulting from the small size and increasing surface-to-volume ratio, which enhances their ability to absorb light and their use in various environmental and medical applications, including antibacterial activities and catalytic systems.

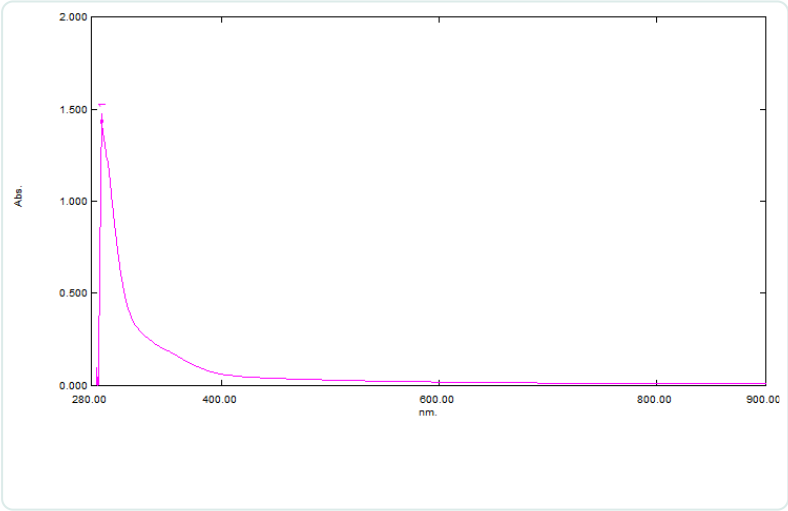

Figure 3. Ultraviolet spectrum of star anise extract with the addition of zinc oxide nanoparticles.

Fourier Transform Infrared Spectroscopy (FTIR) Diagnosis

The Fourier Transform Infrared Spectroscopy (FTIR) analysis of the aqueous extract of star anise treated with zinc oxide nanoparticles revealed several distinct peaks reflecting the chemical reactions occurring during the biosynthesis process. FTIR is used to identify functional groups attached to the surface of nanoparticles, providing clear evidence of their formation and fixation by plant compounds. The zinc oxide nanoparticles (ZnO-NPs) shown in **Figure 4** exhibited a distinct peak in the 500–700 cm^{-1} range, attributed to vibrations resulting from the Zn–O bonds, and constitutes conclusive evidence of zinc oxide nanoparticle formation. The spectrum showed a broad peak in the 3200–3400 cm^{-1} range, attributed to the presence of hydroxyl (OH^-) groups, which may have resulted from water vapor absorption or from phenolic compounds in the star anise extract. Peaks in the 2920–2850 cm^{-1} range indicated the presence of extended C–H bonds, suggesting the persistence of some organic components of the plant extract on the particle surface. Other peaks in the 1700–1600 cm^{-1} range were attributed to the presence of carbonyl or carboxyl (COO^-) groups, which play a role in stabilizing the nanoparticles. These results are consistent with what **(27)** indicated, that the absorption peaks in the 500–700 cm^{-1} range represent the characteristic Zn–O bonds in the metallic nanoparticles, while the broad peaks in the 3200–3400 cm^{-1} range reflect the presence of OH^- groups resulting from the adsorption of water or phenolic compounds in the plant extract, thus confirming the structure of the nanoparticles and the nature of the functional groups associated with them.

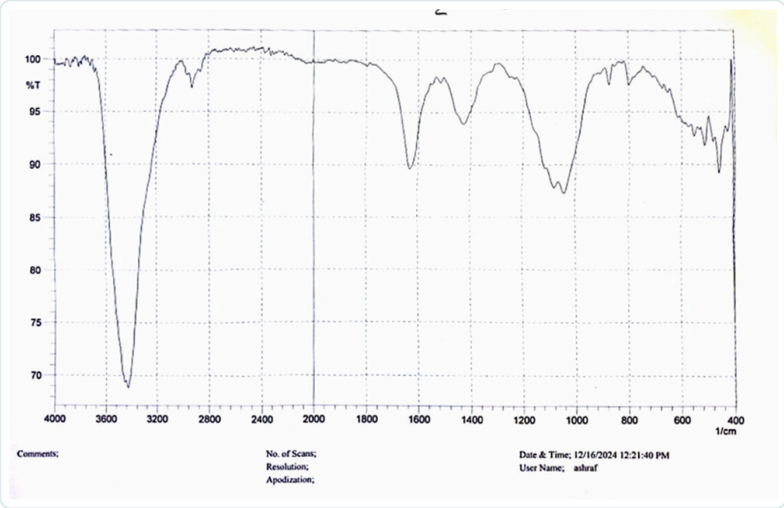

Figure 4. Infrared Spectrum (FTIR) of Star Anise Extract with the addition of zinc oxide nanoparticles.

X-ray Diffraction Microscopy

X-ray diffraction (XRD) analysis of star anise extract treated with zinc oxide nanoparticles revealed distinct crystalline patterns, indicating successful formation of nanoparticles with a defined crystalline structure, as shown in **Figures 5**. XRD is an important tool for determining the crystalline phase, purity, and size of nanocrystals. Since the zinc oxide nanoparticles (ZnO-NPs) (**Figure 5**) concentrated the diffraction pattern at an angle of ~25–30° (2θ), a single, broad, characteristic main peak was observed, located in the (100) crystalline direction. This suggests the formation of quasi-crystalline nanoparticles or very small crystals, as the broadness of the peak indicates the small size of the crystals due to the diffraction of the beam from multiple small surfaces. The absence of additional peaks indicates the purity of the crystal structure and the absence of metallic impurities or secondary compounds. These results suggest that the ZnO particles are smaller and more dispersed in a microcrystalline form. This is attributed to the nature of the interaction between the components of star anise extract and the metal ions, as the type of metal ion influences the crystallization rate and the size of the resulting nuclei. These findings are consistent with those of **(1)**, who observed that biosynthesized ZnO particles exhibited a broad diffraction peak within the 25–30° range due to their small crystal size, reflecting their quasi-crystalline structure.

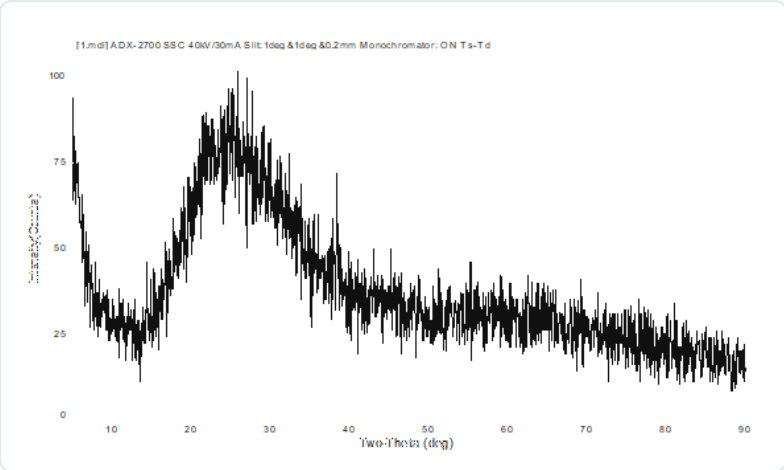

Figure 5. X-ray diffraction of star anise extract with the addition of zinc oxide nanoparticles.

Inhibitory Effect of Star Anise Extract on Isolated Microorganisms from Meat:

Table 5 indicates that the aqueous extract of star anise exhibited varying inhibitory activity against some bacterial species isolated from meat. It showed a clear effect against *Salmonella* and *Escherichia coli* but no effect against *Staphylococcus aureus* and *Pseudomonas aeruginosa*. The inhibition zone diameter for *Salmonella* at concentrations of 125, 250, 500, and 1000 µg/mL were 1.8, 2.0, 3.8, and 3.8 cm, respectively, indicating a dose-dependent increase in inhibition up to 500 µg/mL, after which activity plateaued, suggesting saturation of active compounds. This effect is attributed to phenolic and flavonoid compounds such as anethole in star anise, which disrupt bacterial cell walls and interfere with DNA transcription mechanisms. For *Escherichia coli*, the response was irregular, with inhibition zones of 2.8, 4.0, 2.9, and 4.5 cm at the respective concentrations. This fluctuation may result from variable bacterial cell responses or physical interactions between active compounds and the outer membrane structure. Nonetheless, the highest inhibition at 1000 µg/mL indicates sensitivity at high extract concentrations. The extract showed no activity against *Staphylococcus aureus* and *Pseudomonas aeruginosa*, with zero inhibition zones across all concentrations. This is likely due to the thick cell wall of Gram-positive *S. aureus* and the multi-resistance mechanisms of *P. aeruginosa*, including robust outer membranes and efflux pumps. These findings align with previous research demonstrating that plant extracts' antimicrobial efficacy varies depending on the targeted bacterial species, due largely to differences in cell wall structure affecting susceptibility to active compounds. For example, **(18)** reported that essential oil of star anise exhibited antibacterial activity against *Salmonella* spp. in sous-vide cooked pumpkin models, highlighting its use as a natural preservative in meat products. **(5)** showed that star anise oil possesses broad-spectrum antibacterial activity against *E. coli*, *S. aureus*, and *P. aeruginosa*, attributing its mechanism to disruption of bacterial membranes and interference with vital cellular functions, supporting its application as a microbial contaminant inhibitor in the food industry.Therefore, these results confirm that star anise extract has selective antibacterial properties, with clear efficacy against *Salmonella* and *E. coli* but limited activity against resistant strains such as *S. aureus* and *P. aeruginosa*. It is recommended to explore enhancement techniques such as nanotechnology or combination with other plant extracts to improve its antimicrobial effectiveness.

Table 5. Inhibitory Effect of Star Anise Extract Against Some Bacterial Species Isolated from Meat.

No.	Bacteria	Inhibition zone (cm)			
		Star anise concentration (µg/ml)			
		125 gµ \ml	250 gµ \ml	500 gµ \ml	1000 gµ \ml
1	Salmonella	1.8 a	2.0 a	3.8 a	3.8 a
2	E. coli	2.8 b	4.0 a	2.9 b	4.5 a
3	Staphylococcus aureus	0.0 a	0.0 a	0.0 a	0.0 a
4	Pseudomonas aeruginosa	0.0 a	0.0 a	0.0 a	0.0 a

Different letters in a row indicate significant differences between means at a probability level of 0.05.

Inhibitory Effect of Star Anise Extract Enhanced with Zinc Oxide Nanoparticles on Some Microorganisms Isolated from Meat:

The results presented in **Table 6** demonstrated a clear efficacy of star anise extract enhanced with zinc oxide nanoparticles against multiple bacterial species isolated from meat. The diameters of inhibition zones were measured at four different concentrations (125, 250, 500, 1000 µg/ml). It was found that all bacterial types exhibited varying degrees of inhibitory response, confirming the high efficiency of the plant-nano composite in suppressing microbial growth. These findings are consistent with those reported by **(5)**, who confirmed that reinforcing plant extracts with ZnO nanoparticles enhances their ability to inhibit the growth of various bacteria, including resistant strains. Regarding *Salmonella*, a clear increase in inhibition zone diameter was observed with increasing concentration, reaching values of 2.2, 3.1, 3.5, and 4.6 cm respectively, indicating a positive correlation between nanoparticle concentration and inhibitory efficacy. This effect is attributed to the high capability of ZnO nanoparticles to interact with the bacterial cell wall, causing increased membrane permeability and destruction of essential cellular components. This aligns with **(37)**, who confirmed that the physicochemical properties of nanoparticles contribute to the disruption of fundamental bacterial cell components. As for *Escherichia coli*, it showed a moderate response at lower concentrations (1.3 and 2.5 cm), while the response improved at 500 and 1000 µg/ml (3.0 and 4.0 cm), indicating that the cumulative effect of the plant extract combined with zinc nanoparticles enhances efficacy even against moderately resistant species. Concerning *Staphylococcus aureus*, which showed no response in the previous experiment with the plant extract alone, it exhibited clear positive responses upon enhancement with zinc nanoparticles, with inhibition zones measuring 2.5, 2.4, 3.6, and 4.5 cm respectively. This confirms that nanoparticles improved the penetration of active compounds into the Gram-positive bacterial cells despite the difficulty posed by their thick cell wall. These findings agree with **(26)**, who demonstrated the ability of nanoparticles to bypass cellular barriers in Gram-positive bacteria and improve the permeability of active compounds. *Pseudomonas aeruginosa*, known for its high biological resistance, also showed gradual improvement in response with increasing concentration, with inhibition diameters of 1.0, 2.0, 2.3, and 3.5 cm. This is a strong indicator of the inhibitory efficiency of this nanocomposite system even against resistant bacteria. The formation of clear inhibition halos around the discs is conclusive evidence of the nanocomposite's effectiveness in preventing bacterial growth. This effect is attributed to the unique properties of nanoparticles such as their small size and increased active surface area, which enable them to penetrate the bacterial cell wall and interact with intracellular proteins and enzymes, causing functional disruptions that lead to cell death. Additionally, star anise extract contributes through its phenolic and flavonoid compounds with antibacterial properties. **(17)** confirmed the efficacy of ZnO nanoparticles in inhibiting highly resistant bacteria due to their small particle size and increased surface area, which facilitate penetration of the cell wall and interaction with vital cellular components. These results align with **(43)**, who emphasized that the unique properties of ZnO nanoparticles, including their small size and active surface area, enable enhanced antibacterial activity when combined with plant extracts such as star anise, leading to bacterial cell dysfunction and death. These findings reinforce the effective role of phenolic and flavonoid compounds present in star anise extract in boosting the inhibitory activity when combined with zinc oxide nanoparticles, as demonstrated in several previous studies **(5)(37)(26)(17)(43)**. The results suggest

that using star anise extract enhanced with ZnO nanoparticles is a biologically safe and effective strategy for combating microbes associated with meat contamination, providing a promising natural alternative to conventional antibiotics in food preservation.

Table 6. Inhibitory Effect of Star Anise Extract Enhanced with Zinc Oxide Nanoparticles Against Some Bacterial Species Isolated from Meat.

No.	Bacteria	Star anise complex enriched with nano zinc oxide (µg/mm)			
		125 gµ \ml	250 gµ \ml	500 gµ \ml	1000 gµ \ml
1	Salmonella	2.2 a	3.1 a	3.5 a	4.6 a
2	E. coli	1.3 c	2.5 b	3.0 b	4.0 a
3	Staphylococcus aureus	2.5 c	2.4 c	3.6 b	4.5 a
4	Pseudomonas aeruginosa	1.0 a	2.0 a	2.3 a	3.5 a

Different letters in a row indicate significant differences between means at a probability level of 0.05.

The Antibacterial Activity of Zinc Oxide Nanoparticles Against Certain Bacteria Isolated from Meat:

Table 3 shows the diameters of inhibition zones resulting from the treatment of several bacterial isolates from meat with zinc oxide nanoparticles (ZnO-NPs) at four different concentrations (125, 250, 500, and 1000 µg/ml). The results revealed significant antibacterial activity of these nanoparticles against the tested bacterial species, with variations in sensitivity depending on the bacterial type and the concentration used. For *Salmonella* spp., the inhibition zone measured 1.0 cm at the lowest concentration and increased to 2.5 cm at 250 µg/ml, then slightly decreased to 1.9 cm at 500 µg/ml before reaching the highest value of 4.0 cm at 1000 µg/ml. This fluctuating pattern may be related to the interaction between nanoparticles and the components of the culture medium; however, the final outcome indicates high efficacy at the highest concentration. The antibacterial action of ZnO-NPs is attributed to their ability to penetrate bacterial cell walls, causing internal damage through the release of Zn^{2+} ions and the generation of reactive oxygen species (ROS), which disrupt cellular homeostasis and ultimately lead to cell death. This mechanism explains the superior performance of ZnO-NPs compared to TiO_2-NPs, especially when used in natural antimicrobial systems like plant extracts **(22)**. As for *E. coli*, it exhibited a relatively high sensitivity even at the lowest concentration (4.2 cm), then slightly decreased at intermediate concentrations (2.8 and 3.1 cm), returning to 4.0 cm at the highest concentration. This indicates a strong susceptibility to ZnO-NPs, which can be attributed to the ultra-small particle size that facilitates rapid attachment to the bacterial membrane and disruption of essential biological processes, as reported by **(12)**. Regarding *Staphylococcus aureus*, the inhibition pattern was irregular, with zone diameters of 2.0, 1.8, 3.0, and 2.0 cm at the respective concentrations, showing the best activity at 500 µg/ml. Despite the fluctuations, the presence of an inhibitory effect at all concentrations suggests the ability of ZnO-NPs to penetrate the thick cell wall of Gram-positive bacteria, especially when accompanied by bioactive compounds that enhance penetration. For *Pseudomonas aeruginosa*, a progressively increasing response was observed, with inhibition zones of 1.2, 4.0, 3.6, and 3.8 cm respectively, indicating clear sensitivity to the treatment. This is particularly promising given the resistance of this strain to inhibition. The antibacterial effect is attributed to the large surface area of the ZnO-NPs, which enhances their interaction with the bacterial cell wall and disrupts its essential functions **(22)** demonstrated that ZnO-NPs can effectively inhibit bacterial growth through Zn^{2+} ion release and ROS generation, leading to membrane damage, enzyme disruption, genetic instability, and eventual cell death.

Table 7. Inhibitory activity of zinc oxide nanoparticles against some bacteria isolated from meat

No.	Bacteria	Inhibition zone (cm)			
		Concentration of zinc oxide nanoparticles (µg/mm)			
		125 gµ \ml	250 gµ \ml	500 gµ \ml	1000 gµ \ml
1	Salmonella	1.0 c	2.5 b	1.9 b	4.0 a
2	E. coli	4.2 a	2.8 b	3.1 b	4.0 a
3	Staphylococcus aureus	2.0 b	1.8 b	3.0 a	2.0 b
4	Pseudomonas aeruginosa	1.2 b	4.0 a	3.6 a	3.8 a

Different letters in a row indicate significant differences between means at a probability level of 0.05.

Sensitivity of some types of bacteria isolated from meat to some antibiotics:

The sensitivity of four bacterial strains isolated from meat was assessed using the disk diffusion method on Mueller-Hinton agar. After 24 hours of incubation at 37°C, inhibition zone diameters were measured to evaluate antibiotic effectiveness—larger zones indicating stronger bacterial susceptibility **(21)**. Cefixime (CFM5) showed minimal efficacy: no inhibition for *Salmonella*, and weak activity against *S. aureus* (1.0 cm), *E. coli* (2.0 cm), and *P. aeruginosa* (2.3 cm), indicating limited activity against Gram-negative strains. Cephalexin (CL30) demonstrated broad activity, with strong inhibition of *S. aureus* (4.6 cm) and *Salmonella* (4.5 cm), and good effects on *E. coli* and *Pseudomonas*. These findings align with **(31)**, who also reported its high efficacy against Gram-positive and some Gram-negative bacteria. Bacitracin (B10), usually effective against Gram-positives, unexpectedly inhibited *E. coli* (2.3 cm), with no effect on *Salmonella*, *S. aureus*, or *Pseudomonas*, possibly due to specific strain susceptibility or medium interactions. Cefotaxime (CTX10) had moderate performance: effective against *S. aureus* (3.2 cm), less against *Pseudomonas* (2.0 cm), and minimal for *E. coli* (1.0 cm), with no effect on *Salmonella*. This supports **(33)**, who noted its higher efficacy against Gram-positive bacteria. Amikacin (AK10) was the most potent antibiotic, showing large inhibition zones against all tested bacteria, especially *Salmonella* (4.8 cm) and *Pseudomonas* (4.1 cm). This supports **(16)**, confirming the broad-spectrum power of aminoglycosides. Amoxicillin (AX10) showed weak performance: ineffective against *Salmonella*, with limited inhibition for other strains due to likely β-lactamase resistance. Tetracycline (TE10) showed moderate efficacy, especially against *S. aureus* (3.0 cm), but weaker on *E. coli* (1.3 cm), which is consistent with its protein synthesis inhibition mechanism **(40)**. Penicillin (P10) was effective against *S. aureus* (3.8 cm) and *Salmonella* (3.4 cm), with weak action on *E. coli* (1.1 cm) and none on *Pseudomonas*, confirming its limited use against resistant Gram-negative strains. **(11)** and **(25)** emphasized the need for targeted antibiotic selection due to increasing resistance.

Table 8. Sensitivity of some types of bacteria isolated from meat to some antibiotics.

No.	Antibiotics	Bacteria			
		Salmonella	*E. coli*	*Staphylococcus aureus*	*Pseudomonas aeruginosa*
1	Cefixime (CFM5)	0.0 b	2.0 a	1.0 b	2.3 b
2	Cephalexin (Cl 30)	4.5 a	3.1 a	4.6 a	3.0 a
3	Bacitracin (B 10)	0.0 b	2.3 a	0.0 b	0.0 b
4	Cefotaxime (CTX 10)	0.0 b	1.0 a	3.2 a	2.0 b
5	Amikacin (Ak 10)	4.8 a	3.3 a	3.2 a	4.1 a
6	Amoxicillin (AX 10)	0.0 b	2.3 a	2.5 b	2.8 b
7	Tetracyclin (TE10)	1.5 b	1.3 a	3.0 a	3.2 a
8	Penicillin (P 10)	3.4 a	1.1 a	3.8 a	0.0 b

Different letters in a column indicate significant differences between means at a probability level of 0.05.

Conclusions

We conclude that the green synthesis of zinc oxide nanoparticles demonstrated clear efficacy against multiple types of bacteria isolated from meat. All bacterial species exhibited varying degrees of inhibitory response, confirming the high efficacy of the plant nanoparticle mixture in disrupting microbial growth.

Supplementary Materials:: No Supplementary Materials.

Author Contributions:: Author 1: Methodology, Writing - Preparation of the original draft; Author 1 and Author 2: Writing - Review and Editing. All authors read and approved the published version of the manuscript.

Funding:: This research received no external funding.

Institutional Review Board Statement:: The study was conducted in accordance with the protocol approved by the Department of Food Science, College of Agriculture, Tikrit University.

Informed Consent Statement:: No Informed Consent Statement.

Data Availability Statement:: No Data Availability Statement.

Conflicts of Interest:: The authors declare no conflict of interest.

Acknowledgments:: Non

Disclaimer/Journal's Note:: The statements, opinions, and data contained in all publications are solely those of the individual author(s) and contributor(s) and not of AJAS and/or the editor(s). AJAS and/or the editor(s) disclaim responsibility for any injury to people or property resulting from any ideas, methods, instructions, or products referred to in the content.

References

1. Abd El Hamid, D. K., Desouky, E. M., AbdEllatif, S., Abed, N., and Mahfouz, A. Y. (2024). Green Synthesis and characterization of Titanium Dioxide nanoparticles by Aspergillus Niger DS22 and its potential application in Medical Fields. *Egyptian Journal of Botany*, 64(2): 629-653. https://doi.org/10.21608/ejbo.2024.245157.2550
2. Adzitey, F., Huda, N., and Shariff, A. H. M. (2021). Phenotypic antimicrobial susceptibility of Escherichia coli from raw meats, ready-to-eat meats, and their related samples in one health context. *Microorganisms*, 9(2): 326. https://doi.org/10.3390/microorganisms9020326
3. Altaee, Z., Alzubaidi, L., and Al-Rubeii, A. (2025). Enhanced Antibacterial Activity of Chitosan Nanoparticles Encapsulated in Annatto Seed Extract Against Meat-Borne Bacterial Contamination. *Anbar Journal of Agricultural Sciences*, 23(2): 1325-1342. https://doi.org/10.32649/ajas.2025.189371
4. Alzaben, F., Fat'hi, S., Elbehiry, A., Alsugair, M., Marzouk, E., Abalkhail, A., and Hamada, M. (2022). Laboratory diagnostic methods and antibiotic resistance patterns of Staphylococcus aureus and Escherichia coli strains: an Evolving Human Health Challenge. https://doi.org/10.3390/diagnostics12112645
5. Angane, M., Swift, S., Huang, K., Butts, C. A., and Quek, S. Y. (2022). Essential oils and their major components: An updated review on antimicrobial activities, mechanism of action and their potential application in the food industry. *Foods*, 11(3): 464. https://doi.org/10.3390/foods11030464
6. Atlas, R. M., Brown, A. E., and Parks, L. C. (1995). *Laboratory manual of experimental microbiology*.
7. Barage, S., Lakkakula, J., Sharma, A., Roy, A., Alghamdi, S., Almehmadi, M., and Abdulaziz, O. (2022). Nanomaterial in food packaging: A comprehensive review. *Journal of Nanomaterials*, 2022(1): 6053922. https://doi.org/10.1155/2022/6053922
8. Bashi, A. M., Zobir, M., Zainal, Z., and Tichit, D. (2013). Journal of Solid State Chemistry Synthesis and controlled release properties of 2 , 4 dichlorophenoxy acetate – zinc layered hydroxide nanohybrid. *Journal of Solid-State Chemistry*, 203: 19-24. https://doi.org/10.1016/j.jssc.2013.03.047
9. Brayner, R., Ferrari-Iliou, R., Brivois, N., Djediat, S., Benedetti, M. F., and Fiévet, F. (2006). Toxicological impact studies based on Escherichia coli bacteria in ultrafine ZnO nanoparticles colloidal medium. *Nano Lett*, 6: 866-870. https://doi.org/10.1021/nl052326h
10. Caroling, G., Tiwari, S. K., Ranjitham, A. M., and Suja, R. (2013). Biosynthesis of silver nanoparticles using aqueous broccoli extract-characterization and study of antimicrobial, cytotoxic effects. *Asian J Pharm Clin Res*, 6(4): 165-172. https://doi.org/10.1016/j.heliyon.2023.e19723
11. Cecropin, A. (2023). *In Vivo Pharmacokinetics Of Meropenem Alone And In Combination With Cationic Antimicrobial Peptide, Cecropin A-(1-7) Melittin Against Multi-Drug Resistant Escherichia Coli In Broiler Chicken*. https://doi.org/10.1128/aac.50.4.1251-1256.2006
12. Chakraborty, N., Jha, D., Roy, I., Kumar, P., Gaurav, S. S., Marimuthu, K., and Gautam, H. K. (2022). Nanobiotics against antimicrobial resistance: harnessing the power of nanoscale materials and technologies. *Journal of nanobiotechnology*, 20(1): 375. https://doi.org/10.1186/s12951-022-01573-9
13. Duan, Y., Han, L., Zhang, J., Asahina, S., Huang, Z., Shi, L., and Che, S. (2015). Optically active nanostructured ZnO films. *Angewandte Chemie International Edition*, 54(50): 15170-15175. https://doi.org/10.1002/anie.201507502
14. Duncan, D. B. (1955). Multiple range and multiple F tests. *biometrics*, 11(1): 1-42. https://doi.org/10.1007/978-1-4612-4974-0_38
15. Ezealisiji, K. M., Siwe-Noundou, X., Maduelosi, B., Nwachukwu, N., and Krause, R. W. M. (2019). Green synthesis of zinc oxide nanoparticles using Solanum torvum (L) leaf extract and evaluation of the toxicological profile of the ZnO nanoparticles–hydrogel composite in Wistar albino rats. *International Nano Letters*, 9(2): 99-107. https://doi.org/10.1007/s40089-018-0263-1
16. Farhan, S. M., El-Baky, R. M. A., Abdalla, S., El-Gendy, A. O., Ahmed, H. R., Mohamed, D. S., and Azmy, A. F. (2022). In vitro and in vivo effect of amikacin and imipenem combinations against multidrug-resistant E. coli. *Tropical Medicine and Infectious Disease*, 7(10): 281. https://doi.org/10.3390/tropicalmed7100281
17. Flores-Contreras, E. A., González-González, R. B., Pablo Pizaña-Aranda, J. J., Parra-Arroyo, L., Rodríguez-Aguayo, A. A., Iñiguez-Moreno, M., and Melchor-Martínez, E. M. (2024). Agricultural waste as a sustainable source for nanoparticle synthesis and their antimicrobial properties for food preservation. *Frontiers in Nanotechnology*, 6: 1346069. https://doi.org/10.3389/fnano.2024.1346069

18. Kačániová, M., Vukovic, N. L., Čmiková, N., Bianchi, A., Garzoli, S., Ben Saad, R., and Vukic, M. D. (2024). Biological activity and phytochemical characteristics of star anise (Illicium verum) essential oil and its anti-Salmonella activity on sous vide pumpkin model. *Foods*, 13(10): 1505. https://doi.org/10.3390/foods13101505
19. Kalpana, V. N., and Devi Rajeswari, V. (2018). A review on green synthesis, biomedical applications, and toxicity studies of ZnO NPs. *Bioinorganic chemistry and applications*, 2018(1): 3569758. https://doi.org/10.1155/2018/3569758
20. Karmous, I., Pandey, A., Haj, K. B., and Chaoui, A. (2020). Efficiency of the green synthesized nanoparticles as new tools in cancer therapy: insights on plant-based bioengineered nanoparticles, biophysical properties, and anticancer roles. *Biological trace element research*, 196: 330-342. https://doi.org/10.1007/s12011-019-01895-0
21. Kowalska-Krochmal, Beata, and Dudek-Wicher, Ruth. (2021). The minimum inhibitory concentration of antibiotics: methods, interpretation, clinical relevance. *Pathogens*, 10(2): 165. https://doi.org/10.3390/pathogens10020165
22. Krishnamoorthy, R., Athinarayanan, J., Periyasamy, V. S., Alshuniaber, M. A., Alshammari, G., Hakeem, M. J., and Alshatwi, A. A. (2022). Antibacterial mechanisms of zinc oxide nanoparticle against bacterial food pathogens resistant to beta-lactam antibiotics. *Molecules*, 27(8): 2489. https://doi.org/10.3390/molecules27082489
23. Lee, S. A., and Link, S. (2021). Chemical interface damping of surface plasmon resonances. *Accounts of chemical research*, 54(8): 1950-1960. https://doi.org/10.1021/acs.accounts.0c00872
24. Malka, E., Perelshtein, I., Lipovsky, A., Shalom, Y., Naparstek, L., Perkas, N., and Gedanken, A. (2013). Eradication of multi-drug resistant bacteria by a novel Zn-doped CuO nanocomposite. *Small*, 9(23): 4069-4076. https://doi.org/10.1002/smll.201301081
25. Mancuso, G., Midiri, A., Gerace, E., and Biondo, C. (2021). Bacterial antibiotic resistance: the most critical pathogens. *Pathogens*, 10(10): 1310. https://doi.org/10.3390/pathogens10101310
26. Mushtaq, W., Ishtiaq, M., Maqbool, M., Mazhar, M. W., Casini, R., Abd-ElGawad, A. M., and Elansary, H. O. (2023). Green synthesis of zinc oxide nanoparticles using Viscum album extracts: Unveiling bioactive compounds, antibacterial potential, and antioxidant activities. *Plants*, 12(11): 2130. https://doi.org/10.3390/plants12112130
27. Pasieczna-Patkowska, S., Cichy, M., and Flieger, J. (2025). Application of Fourier Transform Infrared (FTIR) Spectroscopy in Characterization of Green Synthesized Nanoparticles. *Molecules*, 30(3): 684. https://doi.org/10.3390/molecules30030684
28. Pathania, S., Hmar, J. J. L., Verma, B., Majumder, T., Kumar, V., and Chinnamuthu, P. (2022). Titanium dioxide (TiO2) sensitized zinc oxide (ZnO)/conducting polymer nanocomposites for improving performance of hybrid flexible solar cells. *Journal of Electronic Materials*, 51(10): 5986-6001. https://doi.org/10.1007/s11664-022-09815-0
29. Perumalsamy, H., Balusamy, S. R., Sukweenadhi, J., Nag, S., MubarakAli, D., El-Agamy Farh, M., and Rahimi, S. (2024). A comprehensive review on Moringa oleifera nanoparticles: importance of polyphenols in nanoparticle synthesis, nanoparticle efficacy and their applications. *Journal of Nanobiotechnology*, 22(1): 71. https://doi.org/10.1186/s12951-024-02332-8
30. Raedani, T. J. (2023). *Microbial analysis of street vended ready-to-eat meat around Thohoyandou Area, Vhembe District, Limpopo Province, RSA*. https://doi.org/10.1080/23311932.2023.2185965
31. Rahim, S., Perveen, S., Ahmed, S., Shah, M. R., and Malik, M. I. (2020). Enhancement in the antibacterial activity of cephalexin by its delivery through star-shaped poly (ε-caprolactone)-block-poly (ethylene oxide) coated silver nanoparticles. *Royal Society Open Science*, 7(10): 201097. https://doi.org/10.1098/rsos.201097
32. Rajeshkumar, S., Malarkodi, C., Gnanajobitha, G., Paulkumar, K., Vanaja, M., Kannan, C., and Annadurai, G. (2013). Seaweed-mediated synthesis of gold nanoparticles using Turbinaria conoides and its characterization. *Journal of Nanostructure in Chemistry*, 3(1): 44. https://doi.org/10.1186/2193-8865-3-44
33. Sallam, K. I., Abd-Elrazik, Y., Raslan, M. T., Imre, K., Morar, A., Herman, V., and Zaher, H. A. (2023). Cefotaxime-, ciprofloxacin-, and extensively drug-resistant Escherichia coli O157: H7 and O55: H7 in camel meat. *Foods*, 12(7): 1443. https://doi.org/10.3390/foods12071443
34. Sarathi, R., Sheeba, N. L., Essaki, E. S., and Sundar, S. M. (2022). Titanium doped Zinc Oxide nanoparticles: A study of structural and optical properties for photocatalytic applications. *Materials Today: Proceedings*, 64: 1859-1863. https://doi.org/10.1016/j.matpr.2022.06.387
35. Sarwar, A., Katas, H., Samsudin, S. N., and Zin, N. M. (2015). Regioselective sequential modification of chitosan via azide-alkyne click reaction: synthesis, characterization, and antimicrobial activity of chitosan derivatives and nanoparticles. *PLoS One*, 10(4). https://doi.org/10.1371/journal.pone.0123084
36. SAS. (2001). *Version, Statistical Analysis System*. https://doi.org/10.1177/089443939100900418
37. Sharma, M., Bassi, H., Chauhan, P., Thakur, P., Chauhan, A., Kumar, R., and Thakur, N. K. (2022). Inhibition of the bacterial growth as a consequence of synergism of Ag and ZnO: Calendula officinalis mediated green approach for nanoparticles and impact of altitude. *Inorganic Chemistry Communications*, 136: 109131. https://doi.org/10.1016/j.inoche.2021.109131
38. Shedbalkar, U., Singh, R., Wadhwani, S., Gaidhani, S., and Chopade, B. A. (2014). Microbial synthesis of gold nanoparticles: current status and future prospects. *Advances in colloid and interface science*, 209: 40-48. https://doi.org/10.1016/j.cis.2013.12.011
39. Sobhy, A., and Shaltout, F. (2020). Prevalence of some food poisoning bacteria in semi cooked chicken meat products at Kaliobyia governorate with using of recent Vitek 2 compact and PCR techniques. *Benha Veterinary Medical Journal*, 38(2): 88-92. https://doi.org/10.21608/bvmj.2020.25545.1183
40. Truong-Bolduc, Q. C., Wang, Y., and Hooper, D. C. (2022). Role of Staphylococcus aureus Tet38 in transport of tetracycline and its regulation in a salt stress environment. *Journal of Bacteriology*, 204(7): e00142-22. https://doi.org/10.1128/jb.00142-22
41. Ullah, A., and Lim, S. I. (2022). Plant extract-based synthesis of metallic nanomaterials, their applications, and safety concerns. *Biotechnology and Bioengineering*, 119(9): 2273-2304. https://doi.org/10.1002/bit.28148
42. Vandepitte, J., Engback, K., Piot, P., and Henck, C. (1999). *Basic Laboratory Procedures in Clinical Bacteriology*. https://doi.org/10.1016/s0031-3025(16)35813-5
43. Vera, J., Herrera, W., Hermosilla, E., Díaz, M., Parada, J., Seabra, A. B., and Rubilar, O. (2023). Antioxidant activity as an indicator of the efficiency of plant extract-mediated synthesis of zinc oxide nanoparticles. *Antioxidants*, 12(4): 784. https://doi.org/10.3390/antiox12040784
44. Wang, L., Hu, C., and Shao, L. (2017). The antimicrobial activity of nanoparticles: present situation and prospects for the future. *International journal of nanomedicine*: 1227-1249. https://doi.org/10.2147/ijn.s121956
45. Watban, H. M., and Al-Maaly, N. M. (2024). Diagnostic Study of Pathogenic Bacterial Isolated from Camel's Pneumonic lungs Slaughtered in Al-Muthanna Province Abattoir, Iraq Using Vitek2 Compactiological approach and Vitek2 compact in Al-Muthanna province. *The Iraqi Journal of Veterinary Medicine*, 48(2): 113-118. https://doi.org/10.30539/t3h56g72
46. Wilson, A. J., Devasia, D., and Jain, P. K. (2020). Nanoscale optical imaging in chemistry. *Chemical Society Reviews*, 49(16): 6087-6112. https://doi.org/10.1039/d0cs00338g

47. Winn, W. C. (2006). *Koneman's color atlas and textbook of diagnostic microbiology*. https://doi.org/10.1016/0732-8893(85)90044-6

48. Zhang, W., Chou, X., Shi, T., Ma, Z., Bao, H., Chen, J., and Xue, C. (2017). *Measurement technology for micro-nanometer devices*. https://doi.org/10.1002/9781118717974

مقالة أصيلة

التخليق الحيوي لجسيمات الزنك النانوية باستعمال اليانسون النجمي وتقييم فعاليتها المضادة للمايكروبات ضد الميكروبات المعزولة من لحوم الأغنام

سارة سمير داود ، منال صالح مهدي

قسم علوم الأغذية، كلية الزراعة، جامعة تكريت، العراق

البريد الإلكتروني للمراسلة: sd230010pag@st.tu.edu.iq

الخلاصة

أجريت الدراسة في مختبرات قسم علوم الأغذية والمختبر المركزي بكلية الزراعة بجامعة تكريت، وكان الهدف الأساسي منها هو التخليق الحيوي لجسيمات أكسيد الزنك النانوية (ZnO NPs) باستخدام مستخلص نبات اليانسون النجمي (Illicium verum) وتقييم تأثيرها المثبط ضد البكتيريا المسببة للأمراض المنقولة بالغذاء، وهي المكورات العنقودية الذهبية، والإشريكية القولونية، والزائفة الزنجارية، والسالمونيلا. وقد تم التعرف على هذه الكائنات الدقيقة من خلال مجموعة من الاختبارات المورفولوجية والكيميائية الحيوية، بالإضافة إلى تحليل نظام VITEK. وقد تم تأكيد التخليق الأخضر لجسيمات أكسيد الزنك النانوية باستخدام المستخلص المائي لليانسون النجمي من خلال تغير واضح في اللون في خليط التفاعل. وعلى وجه التحديد، في غضون 20 دقيقة من إضافة مادة أكسيد الزنك الأولية إلى المستخلص، تحول لون المحلول من الأصفر إلى البني الفاتح، مما يشير إلى تكوين الجسيمات النانوية. كشف المزيد من التوصيف باستخدام المجهر الإلكتروني الماسح (SEM) أن جسيمات أكسيد الزنك النانوية المُصنّعة حيويًا كانت كروية في الغالب، مع أحجام جسيمات تتراوح بين 25.4 و78.4 نانومتر. كشف تحليل مطيافية الأشعة فوق البنفسجية والمرئية للمستخلص المائي لليانسون النجمي المعالج بجسيمات أكسيد الزنك النانوية عن نمط امتصاص مميز. عند إضافة جسيمات أكسيد الزنك النانوية (ZnO-NPs) إلى اليانسون النجمي، لوحظ نطاق امتصاص يتراوح بين 280 و900 نانومتر، ويبلغ ذروته عند طول موجي يتراوح بين 280 و300 نانومتر بمعدل امتصاص يبلغ حوالي 1.5 وحدة امتصاص. بعد هذا النطاق، انخفض الامتصاص تدريجيًا مع زيادة الطول الموجي، مقتربًا من الصفر بعد 400 نانومتر. أظهر تحليل مطيافية الأشعة تحت الحمراء بتحويل فورييه (FTIR) لنفس المستخلص. كشف تحليل حيود الأشعة السينية (XRD) لمستخلص اليانسون النجمي المعالج بجسيمات أكسيد الزنك النانوية عن أنماط. يشير الهيكل البلوري الواضح إلى تكوين ناجح لجسيمات نانوية ذات بنية بلورية محددة. أظهر المستخلص المائي لليانسون النجمي وحده نشاطًا مضادًا للبكتيريا متفاوتًا ضد البكتيريا المعزولة من اللحوم. أظهر تأثيرات مثبطة ملحوظة على السالمونيلا والإشريكية القولونية، ولكن لم يُلاحظ أي نشاط كبير ضد المكورات العنقودية الذهبية أو الزائفة الزنجارية. كانت مناطق التثبيط للسالمونيلا عند تركيزات 125 و250 و500 و1000 ميكروغرام/مل 1.8 و2.0 و3.8 و3.8 سم على التوالي. أظهر المركب نشاطًا مثبطًا ضد جميع سلالات البكتيريا المختبرة. وتؤكد هذه النتائج الإمكانات العالية المضادة للميكروبات لمزيج النبات والجسيمات النانوية، وخاصة في قمع نمو مسببات الأمراض المرتبطة باللحوم

الكلمات المفتاحية: المركب النانوي، جسيمات الزنك النانوية، اليانسون النجمي، الميكروبات، لحوم الأغنام